

## Pyroelectric response of ferroelectric thin films

A. Sharma, Z.-G. Ban, and S. P. Alpay<sup>a)</sup>

*Department of Metallurgy and Materials Engineering and Institute of Materials Science, University of Connecticut, Storrs, Connecticut 06269*

J. V. Mantese

*Delphi Research Laboratories, Shelby Township, Michigan 48315*

(Received 27 August 2003; accepted 18 December 2003)

A thermodynamic formalism is developed to calculate the pyroelectric coefficients of epitaxial (001)  $\text{Ba}_{0.6}\text{Sr}_{0.4}\text{TiO}_3$  (BST 60/40) and  $\text{Pb}_{0.5}\text{Zr}_{0.5}\text{O}_3$  (PZT 50/50) thin films on (001)  $\text{LaAlO}_3$ ,  $0.29\text{LaAlO}_3:0.35(\text{Sr}_2\text{TaAlO}_6)$  (LSAT), MgO, Si, and  $\text{SrTiO}_3$  substrates as a function of film thickness by taking into account the formation of misfit dislocations at the growth temperature. The role of internal stress is discussed in detail with respect to epitaxy-induced misfit and thermal stresses arising from the difference between the thermal expansion coefficients of the film and the substrates. It is shown that the pyroelectric coefficients steadily increase with increasing film thickness for BST 60/40 and PZT 50/50 on LSAT and  $\text{SrTiO}_3$  substrates due to stress relaxation by misfit dislocations. Large pyroelectric responses ( $\sim 1.1\ \mu\text{C}/\text{cm}^2\text{K}$  for BST 60/40 and  $\sim 0.3\ \mu\text{C}/\text{cm}^2\text{K}$  for PZT 50/50) are theoretically predicted for films on MgO substrates at critical film thicknesses ( $\sim 52\ \text{nm}$  for BST 60/40 and  $\sim 36\ \text{nm}$  for PZT 50/50) corresponding to the ferroelectric to paraelectric phase transformation. Analysis shows that the pyroelectric coefficients of both BST 60/60 and PZT 50/50 epitaxial films on Si substrates are an order of magnitude smaller than corresponding films on  $\text{LaAlO}_3$ , LSAT, MgO, and  $\text{SrTiO}_3$  substrates. © 2004 American Institute of Physics. [DOI: 10.1063/1.1649460]

### I. INTRODUCTION

Application of ferroelectric materials in infrared (IR) detectors continues to be of importance due to their ability to provide economical pyroelectric detectors and thermal imaging devices; attributed to their ability to be used successfully at ambient temperatures, thereby eliminating the need for expensive cooling systems.<sup>1-4</sup> The use of ferroelectric detectors having low thermal mass (thin film form) with small specific heat and high sensitivity, enhances their speed of response. Optimally, it is desirable to produce low cost, compact, sensitive, and fast responding IR detector ferroelectrics as large hybrid arrays of ferroelectric IR detectors coupled with silicon microelectronic elements. In most cases, this requires integration of ferroelectrics in thin film form with Si integrated circuits.<sup>5</sup>

$\text{Ba}_{0.6}\text{Sr}_{0.4}\text{TiO}_3$  (BST 60/40) and  $\text{Pb}_{0.5}\text{Zr}_{0.5}\text{TiO}_3$  (PZT 50/50) are considered leading candidates as the active materials for pyroelectric sensors because these compounds provide a relatively large response at room temperature (RT, 25 °C).<sup>6,7</sup> This is because BST 60/40 undergoes a paraelectric-ferroelectric transition close to RT; likewise, minor additions of elements such as Nb, Ta, and La brings the paraelectric-ferroelectric phase transformation in PZT 50/50 thin films close to RT, thus initiating a nonlinear pyroelectric response at RT for both materials.

The typical pyroelectric coefficient of a ferroelectric single crystal is  $\sim 1\ \mu\text{C}/\text{cm}^2\text{K}$ .<sup>8</sup> However, experimental val-

ues of the pyroelectric coefficient obtained for ferroelectric thin films, as reported in the literature, range between 0.01 to  $0.5\ \mu\text{C}/\text{cm}^2\text{K}$ .<sup>3,6,9,10</sup> The substandard performance of thin film ferroelectric materials is not specific to only the pyroelectric response but to nearly all their electrical and electromechanical properties. Inferior properties of ferroelectric thin films are usually attributed to the presence of microstructural and compositional inhomogeneities, defects, and internal stresses.<sup>11</sup> In homogeneous epitaxial single-domain ferroelectric thin films, internal stresses arise due to a variety of reasons, including the lattice mismatch between the film and the substrate, the difference in thermal expansion coefficients (TECs) of the film and the substrate, the self-strain of the paraelectric-ferroelectric phase transformation if the material is deposited above the phase transformation temperature, defects such as dislocations and vacancies, and dimensional changes in the film caused during the deposition.

The effects of internal stresses on the electrical and electromechanical properties have been experimentally and theoretically investigated for a number of ferroelectric systems. For epitaxial single-domain ferroelectrics<sup>12</sup> and relaxor ferroelectrics<sup>13,14</sup> the role of internal stresses on a variety of physical, electrical, and electromechanical properties were determined experimentally. For (001) BST 60/40 thin films on  $0.29\text{LaAlO}_3:0.35(\text{Sr}_2\text{TaAlO}_6)$  (LSAT) substrates, significant improvement in the dielectric response was observed as a function of increasing film thickness, associated with the relaxation of in-plane compressive stresses via misfit dislocation formation.<sup>15</sup> X-ray diffraction and Raman scattering revealed a shift in the Curie temperature from 17 to 82 °C in heteroepitaxial (001) BST 70/30 thin films deposited on

<sup>a)</sup> Author to whom all correspondence should be addressed; electronic mail: p.alpay@ims.uconn.edu

(001) MgO.<sup>16</sup> The shift of phase transition temperature is attributed to the two-dimensional compressive stresses imposed on the film by the substrate. In another study, a gain of 23% in capacitance after removal of residual stresses in BST 70/30 thin films was observed.<sup>17</sup> Li *et al.*<sup>18</sup> reported an increase in the dielectric constant with increasing in-plane compressive stress, which in turn decreased with increasing thickness of BST 50/50 thin films grown on (001) MgO. At low temperatures, a high value (increase of ~90%) of tunability was observed, attributed to a tensile strain (in the direction of the applied electric field) in epitaxial SrTiO<sub>3</sub> thin films deposited on metal-insulator-oxide Au/SrTiO<sub>3</sub>/SrRuO<sub>3</sub>/LaAlO<sub>3</sub> heterostructures.<sup>19</sup> The electromechanical properties of Pb<sub>1.0</sub>(Nb<sub>0.04</sub>Zr<sub>0.28</sub>Ti<sub>0.68</sub>)O<sub>3</sub> (PNZT) epitaxial films were recently studied and a remarkable recovery in the piezoelectric coefficient associated with the relaxation in internal stresses was theoretically predicted and experimentally verified for ferroelectric “islands” delineated via focused ion-beam milling.<sup>20,21</sup>

Theoretically, the effect of epitaxy-induced internal stresses on the phase transformation characteristics and physical properties has been analyzed using a Landau–Devonshire (LD) thermodynamic model.<sup>22</sup> Using this formalism, the role of internal stresses on the dielectric properties and the tunability of barium strontium titanate films<sup>23,24</sup> as well as the piezoelectric properties of lead zirconate titanate (PZT) epitaxial thin films<sup>25</sup> has been discussed.

In a recent article, we have developed a thermodynamic model to analyze the effect of internal stresses on the pyroelectric response in epitaxial ferroelectric films.<sup>26</sup> Our preliminary findings show that the pyroelectric coefficient is strongly dependent on the misfit strain. A large pyroelectric coefficient of 0.65 μC/cm<sup>2</sup>K was predicted for (001) BST 60/40 at a critical misfit strain of 0.05%. The aim of this article is to extend the theoretical model and analyze the combined effect of the internal stresses due to lattice and thermal expansion mismatch between film and substrate of epitaxial single-domain (001) BST and PZT thin films as a function of film thickness. *Quantitative* estimations of the pyroelectric response for films on different substrates as a function of the film thickness is provided, thereby serving as a guide for the selection of film and substrate materials as well as appropriate growth conditions for future experimental work.

## II. THERMODYNAMIC THEORY

Consider a thin single-domain ferroelectric film that undergoes a cubic [*Pm*3̄*m*] to tetragonal [*P4mm*] phase transformation upon cooling, deposited on a cubic substrate such that (001)<sub>film</sub>//(001)<sub>substrate</sub> at a growth temperature *T<sub>G</sub>* higher than the phase transformation temperature. We define a Cartesian coordinate system with the principal axes *x*<sub>1</sub>//(100)<sub>film</sub>, *x*<sub>2</sub>//(010)<sub>film</sub>, and *x*<sub>3</sub>//(001)<sub>film</sub>. If the thickness of the substrate is much larger than the film thickness, the internal stresses are concentrated in the film and the substrate is stress free. For such a configuration, the LD potential can be expressed in a renormalized form as an expansion in terms of the polarization *P<sub>i</sub>* (*i* = 1, 2, 3 corresponding to

polarization vectors parallel to *x*<sub>1</sub>, *x*<sub>2</sub>, and *x*<sub>3</sub>, respectively), the applied electric field *E<sub>i</sub>* (*i* = 1, 2, 3), and the misfit strain in the *x*<sub>1</sub>–*x*<sub>2</sub> plane, defined as *u<sub>m</sub>* = (*a<sub>S</sub>* – *a*<sub>0</sub>)/*a<sub>S</sub>*, where *a<sub>S</sub>* is the substrate lattice parameter and *a*<sub>0</sub> is the equivalent cubic cell constant of the free standing film, as<sup>22</sup>

$$\begin{aligned} \tilde{G} = & a_1^*(P_1^2 + P_2^2) + a_3^*P_3^2 + a_{11}^*(P_1^4 + P_2^4) + a_{33}^*P_3^4 \\ & + a_{13}^*(P_1^2P_3^2 + P_2^2P_3^2) + a_{12}^*P_1^2P_2^2 + a_{111}(P_1^6 + P_2^6 + P_3^6) \\ & + a_{112}[(P_1^4(P_2^2 + P_3^2) + P_3^4(P_1^2 + P_2^2) + P_2^4(P_1^2 + P_3^2)] \\ & + a_{123}P_1^2P_2^2P_3^2 + \frac{u_m^2}{S_{11} + S_{12}}(E_1P_1 + E_2P_2 + E_3P_3). \end{aligned} \quad (1)$$

The renormalized expansion coefficients of the free energy functional are

$$\begin{aligned} a_1^* = & a_1 - u_m \frac{Q_{11} + Q_{12}}{S_{11} + S_{12}}, \quad a_3^* = a_1 - u_m \frac{2Q_{12}}{S_{11} + S_{12}}, \\ a_{11}^* = & a_{11} + \frac{1}{2} \frac{1}{S_{11}^2 - S_{12}^2} [(Q_{11}^2 + Q_{12}^2)S_{11} \\ & - 2Q_{11}Q_{12}S_{12}], \quad a_{33}^* = a_{11} + \frac{Q_{12}^2}{S_{11} + S_{12}}, \quad (2) \\ a_{12}^* = & a_{12} - \frac{1}{S_{11}^2 - S_{12}^2} [(Q_{11}^2 + Q_{12}^2)S_{12} - 2Q_{11}Q_{12}S_{11}] \\ & + \frac{Q_{44}^2}{2S_{44}}, \quad a_{13}^* = a_{12} + \frac{Q_{12}(Q_{11} + Q_{12})}{S_{11} + S_{12}}. \end{aligned}$$

where *a*<sub>1</sub> is the dielectric stiffness, *a<sub>ij</sub>* and *a<sub>ijk</sub>* are higher order stiffness coefficients at constant stress, *Q<sub>ij</sub>* are the electrostrictive coefficients, and *S<sub>ij</sub>* the elastic compliances of the film (the tensor quantities are in the contracted notation throughout). The temperature dependence of the dielectric stiffness *a*<sub>1</sub> is given by the Curie–Weiss law, *a*<sub>1</sub> = (*T* – *T<sub>C</sub>*)/2ε<sub>0</sub>*C*, where *T<sub>C</sub>* and *C* are the Curie–Weiss temperature and constant of a bulk ferroelectric, respectively, and ε<sub>0</sub> is the permittivity of free space. The parameters used for calculating the renormalized coefficients are listed in Tables I and II for BST 60/40 and PZT 50/50.<sup>23,25,27</sup>

TABLE I. The parameters for the calculation of renormalized coefficients. Data compiled from Refs. 22–27. *T<sub>C</sub>*: Curie temperature, *C*: Curie constant, *a<sub>ij</sub>*: stiffness coefficients, *S<sub>ij</sub>*: elastic compliances, and *Q<sub>ij</sub>*: electrostrictive coefficients.

	BST 60/40	PZT 50/50
<i>T<sub>C</sub></i> (°C)	5	392.6
<i>C</i> (10 <sup>5</sup> °C)	1.22	4.247
<i>a</i> <sub>11</sub> (10 <sup>6</sup> m <sup>5</sup> /C <sup>2</sup> F)	2.16 <i>T</i> + 462( <i>T</i> in °C)	4.764
<i>a</i> <sub>12</sub> (10 <sup>8</sup> m <sup>5</sup> /C <sup>2</sup> F)	7.98	1.735
<i>S</i> <sub>11</sub> (10 <sup>–12</sup> m <sup>2</sup> /N)	5.12	10.5
<i>S</i> <sub>12</sub> (10 <sup>–12</sup> m <sup>2</sup> /N)	–1.65	–3.7
<i>S</i> <sub>44</sub> (10 <sup>–12</sup> m <sup>2</sup> /N)	5.86	28.7
<i>Q</i> <sub>11</sub> (m <sup>4</sup> /C <sup>2</sup> )	0.1	0.0966
<i>Q</i> <sub>12</sub> (m <sup>4</sup> /C <sup>2</sup> )	–0.034	–0.046
<i>Q</i> <sub>44</sub> (m <sup>4</sup> /C <sup>2</sup> )	0.029	0.0819

TABLE II. Lattice parameters and respective TECs of BST 60/40 and PZT 50/50 and substrates at RT (from Refs. 23, 25, and 27).

Film/Substrate	Lattice parameter (nm)	TEC ( $\times 10^{-6} \text{ }^\circ\text{C}$ )
BST 60/40	0.3960	10.50
PZT 50/50	0.40155	7.26
LaAlO <sub>3</sub>	0.3787	10.00
LSAT	0.3865	11.00
MgO	0.4211	13.47
SrTiO <sub>3</sub>	0.3904	11.00
Si	0.5431	2.60

The formation of six distinct phases due to the change in the symmetry as a result of the mechanical boundary conditions is predicted theoretically, compared to only three phases in single crystals.<sup>22</sup> These six phases are the *paraelectric* phase ( $P_1 = P_2 = P_3 = 0$ ), the *c*-phase ( $P_1 = P_2 = 0, P_3 \neq 0$ ), the *a*-phase ( $P_1 \neq 0, P_2 = P_3 = 0$ ), the *ac*-phase ( $P_1 \neq 0, P_2 = 0, P_3 \neq 0$ ), the *aa*-phase ( $P_1 = P_2 \neq 0, P_3 = 0$ ), and the *r*-phase ( $P_1 = P_2 \neq 0, P_3 \neq 0$ ). The unusual phases (the *a*-phase, *aa*-phase, *ac*-phase, and *r*-phase) are in essence orientational variants of the tetragonal and the orthorhombic ferroelectric phases that are observed in bulk BaTiO<sub>3</sub> ceramics and single-crystals in succession with decreasing temperature with the exception of the *r*-phase. The *c*- and *a*-phases are tetragonal (space group  $P4mm$ ), the *aa*- and *ac*-phases are orthorhombic (space group  $Amm2$ ) and the *r*-phase is monoclinic (space group  $Pm$ ) compared to the rhombohedral phase with  $P_1 = P_2 = P_3 \neq 0$  (space group  $R3m$ ).

In Fig. 1, we present the temperature-misfit strain phase diagrams for BST 60/40 and PZT 50/50 epitaxial films. The details regarding the construction of these phase diagrams are discussed elsewhere.<sup>22,23,25</sup> The stable phases in BST 60/40 films at RT are the *c*-phase, the *paraelectric* phase, and the *aa*-phase [Fig. 1(a)]. In the case of PZT 50/50 films, the stable phases at RT are the *c*-phase, the *r*-phase, and the *aa*-phase [Fig. 1(b)].

At RT, bulk BST 60/40 is paraelectric and does not exhibit spontaneous polarization while PZT 50/50 is ferroelectric; however for the latter, the crystal structure of the ferroelectric PZT phase is still not completely understood.<sup>25,28,29</sup> According to theoretical predictions, epitaxial films of BST 60/40, however, may be ferroelectric depending on the misfit strain as shown in Fig. 1(a). Similarly, for epitaxial PZT 50/50 films, internal stresses may result in

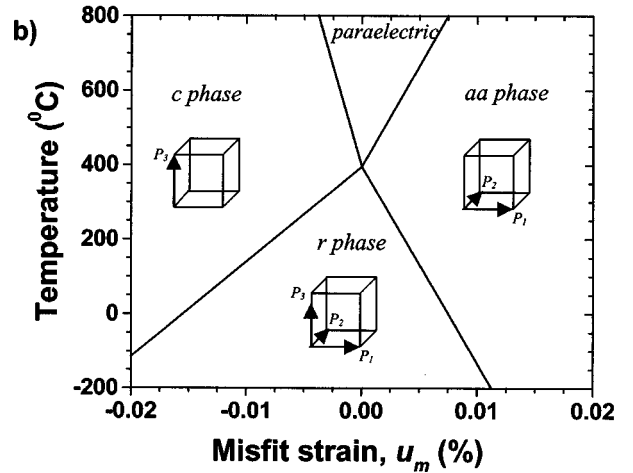
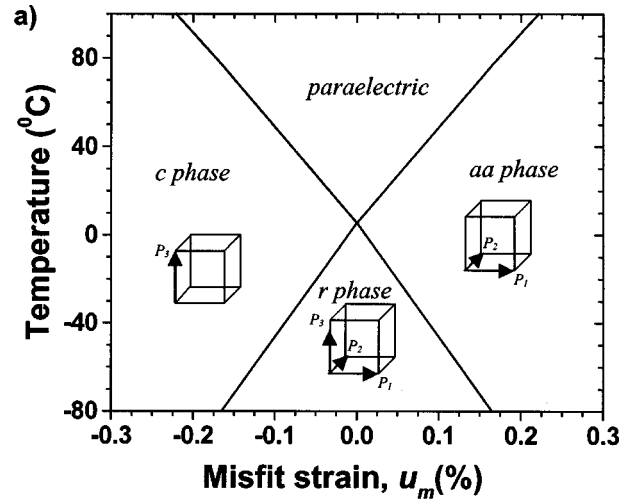


FIG. 1. Phase diagrams of (a) (001) single-domain BST 60/40 and (b) PZT 50/50 epitaxial films on a cubic substrate.

the reorientation of the spontaneous polarization vector, giving rise to a series of phase transitions from the *c*-phase to the *aa*-phase with increasing misfit strain [see Fig. 1(b)].

The polarization component perpendicular to the film-substrate interface may be obtained by minimizing Eq. (1) with respect to out-of-plane polarization,  $P_3 = P_S$

$$c\text{-phase: } P_S = \sqrt{-a_3^*/2a_{33}^*}, \quad (3)$$

$$ac\text{-phase: } P_S = \sqrt{(2a_{11}^*a_3^* - a_{13}^*a_1^*)/(a_{13}^{*2} - 4a_{11}^*a_{33}^*)}, \quad (4)$$

$$r\text{-phase: } P_S = \sqrt{(2a_{13}^*a_1^* - 2a_{11}^*a_3^* - a_{12}^*a_3^*)/(4a_{11}^*a_{33}^* + 2a_{12}^*a_{33}^* - 2a_{13}^{*2})}. \quad (5)$$

In the presence of a uniform applied electric field  $E_3$  normal to the film substrate interface, the pyroelectric response  $p$  along the  $x_3$ -direction is given as the sum of the variation of the spontaneous polarization and the dielectric permittivity  $\epsilon$  along  $x_3$  with the temperature<sup>4</sup>

$$p = \left( \frac{\partial D}{\partial T} \right)_E = \frac{\partial P_S}{\partial T} + E \frac{\partial \epsilon}{\partial T}, \quad (6)$$

where  $D$  is the dielectric displacement.

For the  $c$ -phase

$$\frac{\partial P_S}{\partial T} = -\frac{\sqrt{2}}{4} (-a_3^* a_{33}^*)^{-1/2} \left( a_{33}^* \frac{\partial a_3^*}{\partial T} - a_3^* \frac{\partial a_{33}^*}{\partial T} \right), \quad (7)$$

for the  $ac$ -phase

$$\begin{aligned} \frac{\partial P_S}{\partial T} = & \frac{1}{2} [(2a_{11}^* a_3^* - a_1^* a_{13}^*)(a_{13}^{*2} - 4a_{11}^* a_{33}^*)^3]^{-1/2} \\ & \times \left\{ (a_{13}^{*2} - 4a_{11}^* a_{33}^*) \left[ 2a_3^* \frac{\partial a_{11}^*}{\partial T} + 2a_{11}^* \frac{\partial a_3^*}{\partial T} \right. \right. \\ & \left. \left. - a_{13}^* \frac{\partial a_1^*}{\partial T} \right] - 4(2a_{11}^* a_3^* - a_{13}^* a_1^*) \right. \\ & \left. \times \left[ a_{33}^* \frac{\partial a_{11}^*}{\partial T} + a_{11}^* \frac{\partial a_{33}^*}{\partial T} \right] \right\} \end{aligned} \quad (8)$$

and for the  $r$ -phase

$$\begin{aligned} \frac{\partial P_S}{\partial T} = & \frac{1}{2} [(2a_1^* a_{13}^* - 2a_{11}^* a_3^* - a_{12}^* a_3^*)(2a_{11}^* a_{33}^* + a_{12}^* a_{33}^* \\ & - a_{13}^{*2})^3]^{-1/2} \left\{ (2a_{11}^* a_{33}^* + a_{12}^* a_{33}^* - a_{13}^{*2}) \right. \\ & \times \left[ 2a_{13}^* \frac{\partial a_1^*}{\partial T} - 2a_3^* \frac{\partial a_{11}^*}{\partial T} - (2a_{11}^* + a_{12}^*) \frac{\partial a_3^*}{\partial T} \right] \\ & - (2a_1^* a_{13}^* - 2a_{11}^* a_3^* - a_{12}^* a_3^*) \left[ (2a_{11}^* + a_{12}^*) \frac{\partial a_{33}^*}{\partial T} \right. \\ & \left. \left. + 2a_{33}^* \frac{\partial a_{11}^*}{\partial T} \right] \right\}. \end{aligned} \quad (9)$$

The out-of-plane dielectric permittivity in the presence of  $E_3$  is

$$\epsilon(E_3) = \left( \frac{\partial^2 \tilde{G}}{\partial P_3^2} \right)^{-1} = \frac{1}{2[a_3^* + a_{13}^*(P_1^2 + P_2^2) + 6a_{33}^* P_3^2]}, \quad (10)$$

where the components of the spontaneous polarization are given by the equations of the state,  $\partial \tilde{G} / \partial P_i = 0$ , such that

$$\frac{\partial \tilde{G}}{\partial P_1} = 2(a_1^* + a_{13}^* P_3^2 + a_{12}^* P_2^2) P_1 + 4a_{11}^* P_1^3 - E_1 = 0, \quad (11)$$

$$\frac{\partial \tilde{G}}{\partial P_2} = 2(a_1^* + a_{13}^* P_3^2 + a_{12}^* P_1^2) P_2 + 4a_{11}^* P_2^3 - E_2 = 0, \quad (12)$$

$$\frac{\partial \tilde{G}}{\partial P_3} = 2[a_3^* + a_{13}^*(P_1^2 + P_2^2)] P_3 + 4a_{33}^* P_3^3 - E_3 = 0. \quad (13)$$

TABLE III. Critical thickness for dislocation formation of BST 60/40 and PZT 50/50 films on different substrates.

Substrate material	Critical thickness for dislocation formation (nm)	
	BST 60/40	PZT 50/50
LaAlO <sub>3</sub>	2.6	1.40
LSAT	2.0	2.92
MgO	1.5	2.91
SrTiO <sub>3</sub>	11.8	4.45
Si	1	1

### III. RESULTS AND DISCUSSION

In epitaxial films, the magnitude of the internal stress is a function of the film thickness  $h$ . This is due to the relaxation of lattice mismatch-induced stresses by the formation of misfit dislocations during the film growth. Based on a thermodynamic model, Matthews and Blakeslee<sup>30</sup> predict a critical film thickness  $h_\rho$  corresponding to the onset of misfit dislocations. At the deposition temperature  $T_G$ , the equilibrium linear misfit dislocation density  $\rho$  is given as<sup>15</sup>

$$\rho = \frac{u_m(T_G)}{a_0(T_G)} \left( 1 - \frac{h_\rho}{h} \right), \quad (14)$$

where  $h$  is the film thickness. If no additional dislocations form during cooling, then an ‘‘effective’’ substrate lattice parameter,  $\bar{a}_S$  can be defined as

$$\bar{a}_S = \frac{a_S(T)}{\rho a_S(T) + 1}, \quad (15)$$

which can then be used to calculate the misfit strain instead of the actual lattice parameter.

To study the pyroelectric effect of different substrates with varying film thickness the following substrates were chosen: LaAlO<sub>3</sub>, LSAT, MgO, SrTiO<sub>3</sub>, and Si. Table II lists the lattice parameters and TECs of film and substrate materials at RT. Deposition temperatures are taken as 800 and 600 °C for BST 60/40 and PZT 50/50 thin films, respectively. For BST 60/40 and PZT 50/50, the theoretical Matthews–Blakeslee critical thickness is calculated for the five substrates and is listed in Table III. Figures 2(a) and 2(b) show the misfit strain as a function of the film thickness for BST 60/40 and PZT 50/50 films, respectively. For all cases, a steep decrease in the magnitude of strain is predicted due to the formation of misfit dislocations at the critical thickness. LaAlO<sub>3</sub>, LSAT, and SrTiO<sub>3</sub> exert compressive stresses while MgO and Si exerts tensile stresses on pseudomorphic films. With increasing film thickness, the magnitude of the internal stresses is reduced significantly to a level corresponding to a remnant stress state determined by the TEC difference.

Figures 3(a) and 3(b) reveal the behavior of out-of-plane spontaneous polarization as a function of film thickness for BST 60/40 and PZT 50/50 thin films. A large drop in spontaneous polarization is predicted at the critical film thickness for BST and PZT thin films on LaAlO<sub>3</sub>, LSAT, and SrTiO<sub>3</sub> substrates. This is due to the relaxation in the magnitude of the compressive stress experienced by various substrates. For substrates exerting compressive stresses, the calculated value

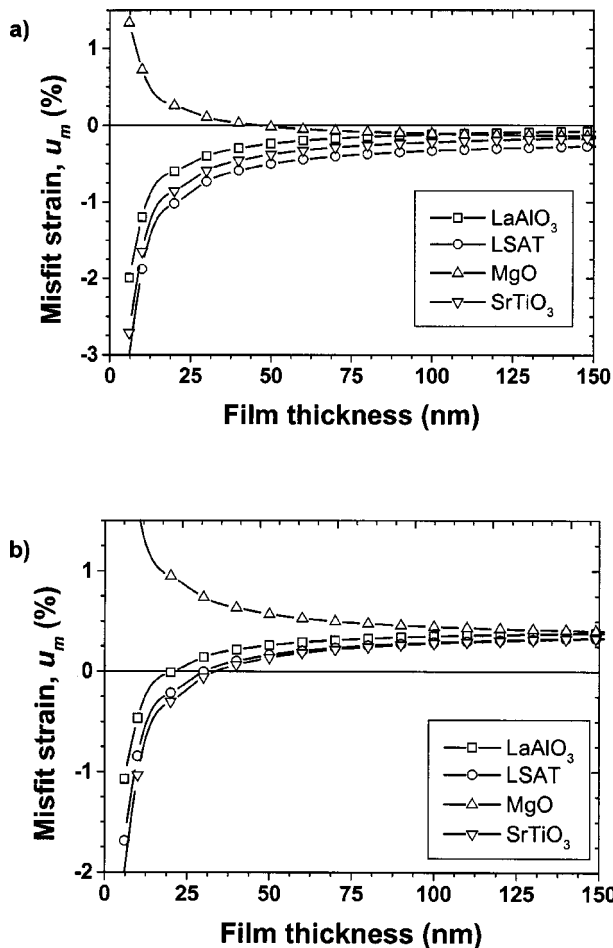


FIG. 2. Variation of misfit strain as a function of film thickness at room temperature (RT=25 °C) for (a) BST 60/40, and (b) PZT 50/50.

of the out-of-plane spontaneous polarization for PZT 50/50 for ultra-thin films ( $\sim 10$  nm) is more than the bulk value of spontaneous polarization. This is in agreement with the experimental values reported by Foster *et al.*,<sup>31</sup> thus substantiating the enhancing role of compressive strain on the polarization in epitaxial films. Close examination of Figs. 3(a) and 3(b) further reveals that in the case of MgO as the substrate, there is no out-of-plane spontaneous polarization up to a certain thickness (52 nm for BST 60/40 and 35 nm for PZT 50/50), after which a steep rise is expected. This is due to the interplay between the relaxation by misfit dislocations and the thermal stresses. Initially, tensile stresses are dominant due to the larger lattice parameter of MgO compared to BST 60/40 and PZT 50/50. But after the formation of misfit dislocations, tensile stresses due to the lattice mismatch are relaxed and compressive stresses due to difference in TECs dominate, resulting in a net compressive stress at RT, which in turn generates an out-of-plane spontaneous polarization. Figure 3(a) also shows a state of zero out-of-plane spontaneous polarization in BST 60/40 on a LaAlO<sub>3</sub> substrate after a thickness of  $\sim 250$  nm. This can be explained by similar arguments as in the case of MgO, but here the TEC difference between film and substrate generates tensile stresses compared to the initial compressive lattice mismatch. Thus, as the film thickness increases, the resulting compressive

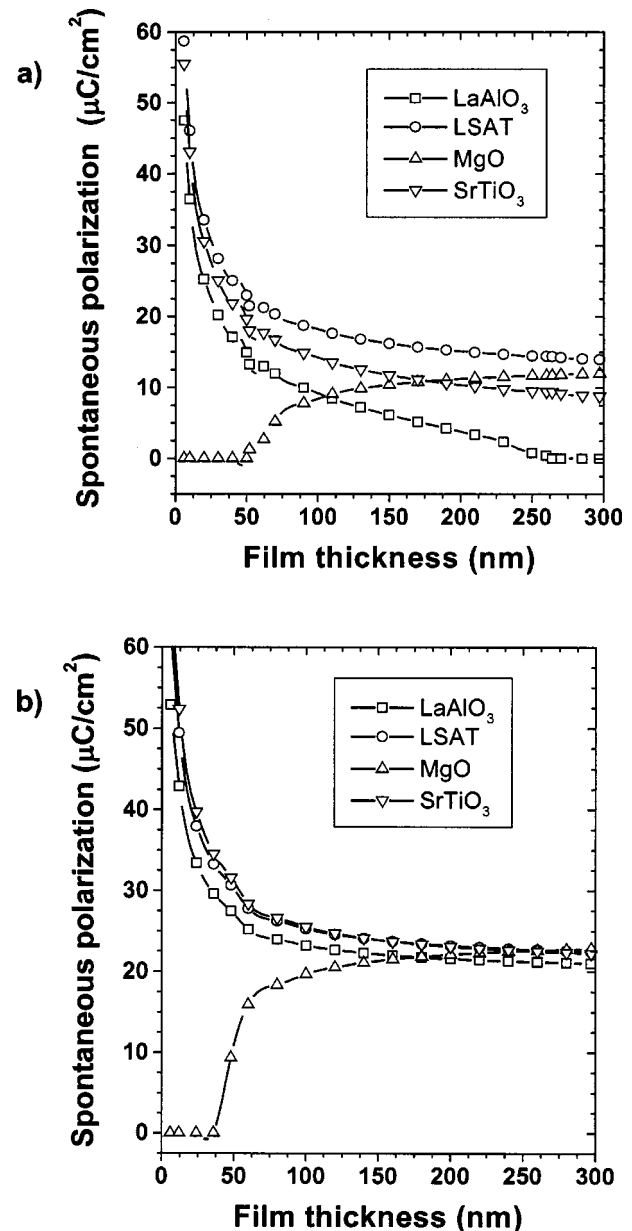


FIG. 3. Spontaneous out-of-plane polarization as a function of film thickness for (001) single-domain (a) BST 60/40 and (b) PZT 50/50 films.

misfit strain decreases below  $\sim 0.05\%$  at which there is a phase transition from the *c*-phase to the *paraelectric* phase, thereby resulting in zero out-of-plane spontaneous polarization.

The pyroelectric response of BST 60/40 and PZT 50/50 films on various substrates as a function of film thickness are shown in Figs. 4(a) and 4(b), respectively, with an applied electric field  $E_3 = 10$  kV/cm. The pyroelectric coefficient is calculated via Eqs. (6)–(13), taking into account the temperature dependence of both the spontaneous polarization and the dielectric constant in the presence of an applied field. It should be noted that the role of the applied electric field to the overall pyroelectric coefficient is relatively small due to the overwhelming contribution of the spontaneous polarization within the stability regions of the ferroelectric phases. For BST 60/40 thin films on LSAT and SrTiO<sub>3</sub> substrates,

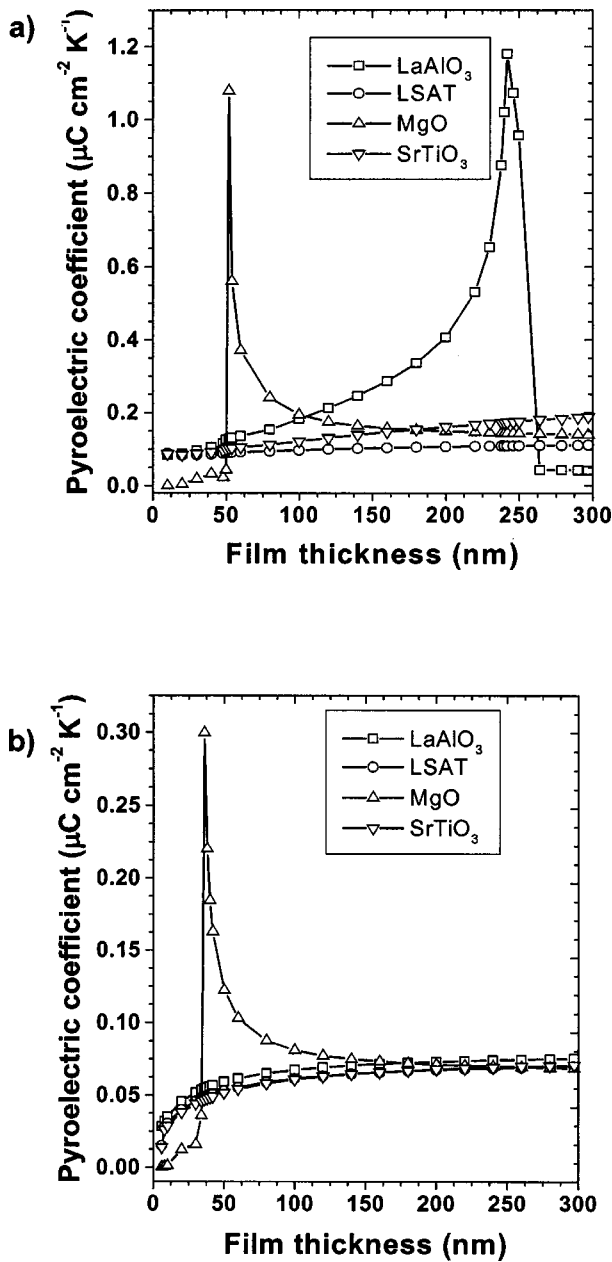


FIG. 4. Pyroelectric coefficient as a function of film thickness on various substrates for (a) BST 60/40 and (b) PZT 50/50 films.

the pyroelectric coefficient increases with increasing film thickness. The interplay between the stress relaxation by misfit dislocations and the thermal stresses that develop during cooling from the deposition temperature results in a change in the stress state at a certain critical film thickness in BST 60/40 films on MgO (~52 nm) and LaAlO<sub>3</sub> (~264 nm) substrates and in PZT 50/50 on MgO (~36 nm) substrates. The change in the stress state gives rise to a *c*-phase ↔ *paraelectric* phase and *c*-phase ↔ *r*-phase transformation for BST 60/40 and PZT 50/50 films, respectively [see Figs. 1(a) and 1(b)], reflected as anomalies in the pyroresponse as shown in Figs. 4(a) and 4(b). Therefore, significant enhancement in the pyroresponse should be expected in BST 60/40 on MgO and LaAlO<sub>3</sub> and PZT 50/50 on MgO in the vicinity of the critical film thickness. The pyroelectric response of

BST 60/40 on MgO is relatively weak below 52 nm since the misfit strain is tensile and thus there is no out-of-plane component of the spontaneous polarization. Pyroelectric coefficients for BST 60/40 and PZT 50/50 thin films were also calculated with (001) Si as the substrate. However, due to large difference in the lattice parameters and TECs of Si and BST 60/40 and PZT 50/50 (Table II), there are high tensile stresses within these films resulting in no contribution by the out-of-plane spontaneous polarization to the pyroelectric response. The pyroresponse of BST 60/40 and PZT 50/50 on Si (not included) increases with film thickness, leveling off at around 250 nm corresponding to the maximum relaxation by misfit dislocations. The behavior is quite similar to BST 60/40 on SrTiO<sub>3</sub> substrate but with a typical pyroresponse in the range of 0.001–0.004  $\mu\text{C/cm K}$  depending on the film thickness.

The theoretical values of pyroelectric coefficient are in agreement with typical experimental values. In particular, the calculated value of pyroelectric coefficient for BST 60/40 films is around 0.2  $\mu\text{C/cm K}$  for relatively thick films ( $h > 150$  nm) at RT except on LaAlO<sub>3</sub>. This is in agreement with the experimentally reported values of 0.18  $\mu\text{C/cm K}$  for 550 nm thick BST 64/36 films deposited on Pt at 30 °C.<sup>9</sup> For PZT 50/50, the theoretical value of pyroelectric coefficient is around 0.07  $\mu\text{C/cm K}$  for relatively thick films ( $h > 150$  nm) which compares well with experimentally reported values of 0.06  $\mu\text{C/cm K}$  for 1  $\mu\text{m}$  thick PZT 50/50 on Pt/Ti/SiO<sub>2</sub><sup>10</sup> and 0.04  $\mu\text{C/cm K}$  for 550 nm thick PZT 30/70 on Pt/Ti/Si<sub>3</sub>N<sub>4</sub>/SiO<sub>2</sub>/Si(100) at RT.<sup>6</sup>

It should be noted that there would be a shift in the phase transformation temperature (compared to the material in single-crystal form) from the cubic *paraelectric* phase to the tetragonal ferroelectric *c*-phase as a result of the internal stresses. The shift in the Curie temperature  $\Delta T_C = T - T_C$  as a function of the misfit strain is given by

$$\Delta T_C = u_m \frac{4Q_{12}}{S_{11} + S_{12}} \epsilon_0 C, \quad (16)$$

which can be obtained by setting  $a_3^* = 0$  in Eq. (2). Accordingly, compressive in-plane strains should stabilize the ferroelectric phase at RT by shifting the transition temperature to higher temperatures ( $\Delta T_C > 0$  since both  $u_m < 0$  and  $Q_{12} < 0$ ). Tensile in-plane strains should result in the lowering of the transformation temperature and thus stabilizing the *paraelectric* phase. Considering that the pyroresponse is the highest at a temperature in the vicinity of the phase transformation temperature, it is also possible to obtain enhanced pyroresponse by varying the operating temperature. In addition, the transformation temperature is a strong function of the film thickness since the extent of reduction in  $u_m$  via misfit dislocation formation depends on the film thickness. These aspects will be discussed in detail in a future article.

In order to emphasize the importance of the thermal stresses that result due to the TEC mismatch, consider a highly (001)-oriented polycrystalline film on a cubic substrate. If the grain size  $D$  is equal to or smaller than the film thickness  $h$ , internal stresses due to lattice mismatch between the film and the substrate are relatively small and can be

neglected. As the film is cooled from  $T_G$ , however, thermal stresses develop. The thermodynamic potential in Eq. (1) for this case is reduced to a relatively simpler form

$$\tilde{G} = a_3^* P_3^2 + a_{33}^* P_3^4 + a_{111} P_3^6 + \frac{u_T^2}{S_{11} + S_{12}} - E_3 P_3, \quad (17)$$

describing the phase transformation characteristics of only the cubic *paraelectric* phase and the tetragonal ferroelectric *c*-phase. Other phases are unlikely to form, as this would be energetically unfavorable. In particular, a rotation of the polarization vector would result in electrically charged grain boundaries creating depoling fields as well as elastic fields due to the electrostrictive coupling between the polarization and the strain. In the above expression,  $u_T$  is the strain due to thermal expansion mismatch, given by:

$$u_T = (\alpha_{\text{film}} - \alpha_{\text{substrate}}) \cdot \Delta T, \quad (18)$$

where  $\alpha_{\text{film}}$  and  $\alpha_{\text{substrate}}$  are the TECs of the film and substrate, respectively, and  $\Delta T$  is the difference between deposition temperature  $T_G$  and RT. The renormalized coefficients are given by Eq. (2), substituting  $u_T$  for  $u_M$ .

Figures 5(a) and 5(b) show the out-of-plane spontaneous polarization calculated for BST 60/40 and PZT 50/50 polycrystalline films on various substrates as a function of deposition temperature,  $T_G$ , respectively. For (001)-textured BST 60/40 polycrystalline thin films on various substrates only MgO substrate exerts significant compressive thermal stresses to generate out-of-plane polarization during cooling to RT. Because of this reason, the pyroelectric coefficient of BST 60/40 is considerably higher on MgO compared to LaAlO<sub>3</sub>, LSAT, and Si substrates, for which there is only a contribution from the temperature dependence of the dielectric constant to the pyroelectric response. For (001)-oriented PZT 50/50 polycrystalline thin films, compressive thermal stresses are generated when the film is deposited on LaAlO<sub>3</sub>, LSAT, and MgO. Thus, the out-of-plane polarization contributes significantly to pyroelectric response of PZT 50/50 on LaAlO<sub>3</sub>, LSAT, and MgO substrates. It should be noted that since the TEC of SrTiO<sub>3</sub> is the same as that of LSAT (Table II), pyroelectric response of polycrystalline BST 60/40 and PZT 50/50 films on SrTiO<sub>3</sub> is expected to be the same as those grown on LSAT under similar conditions.

The limitations of this theoretical approach have been discussed in detail elsewhere.<sup>23</sup> One of the primary parameters of the analysis is the critical film thickness for dislocation formation. The misfit dislocation model of Matthews and Blakeslee is the result of a thermodynamic formalism and thus the real critical thickness for dislocation formation and the linear equilibrium dislocation density may differ significantly from the actual observed values because of kinetic factors controlled by how the misfit dislocations are generated at the interface. A variation in the critical thickness for misfit dislocation generation should in turn alter the critical thickness for maximum pyroresponse [Figs. 4(a) and 4(b)] but not the value of the critical misfit strain corresponding to the *c*-phase ↔ *paraelectric* phase and *c*-phase ↔ *r*-phase transitions for BST 60/40 and PZT 50/50 films, respectively [see Figs. 1(a) and 1(b)].

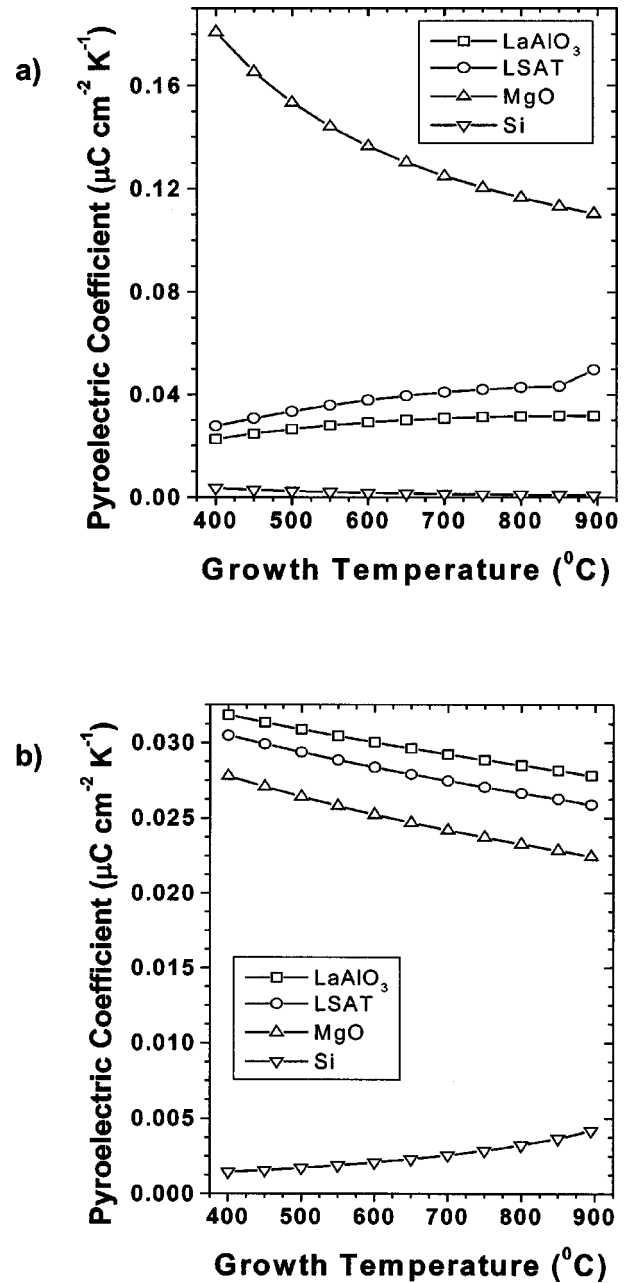


FIG. 5. Pyroelectric coefficient for (a) BST 60/40 and (b) PZT 50/50 polycrystalline thin films on various substrates as a function of growth temperature  $T_G$ .

It should be noted that the developed model could be adapted to describe inhomogeneous distribution of the polarization due to surface effects as well as compositional variations by adding a gradient (Ginzburg) term of the form  $A_{ijkl}(\nabla_i P_j \cdot \nabla_k P_l)$  to Eq. (1). This term represents an additional energy from the nonuniform distribution of the polarization and serves to damp out spatial variations in polarization.<sup>32,33</sup> For gradients in only one direction, the Ginzburg term is reduced to  $A(dP/dz)^2$  and the coefficient  $A$  can be approximated as  $\delta^2|\alpha|$ , where  $\delta$  is the characteristic length along which the polarization varies.

#### IV. SUMMARY AND CONCLUSIONS

In summary, a theoretical formalism was used to understand the combined effect of lattice misfit and thermal

stresses on the pyroelectric response of single-domain ferroelectric thin films. Based on a modified LD phenomenological analysis, the pyroelectric coefficient as a function of film thickness was quantitatively calculated for BST 60/40 and PZT 50/50 on various substrates taking into account the stress relaxation via the formation of the misfit dislocation at growth temperature. The pyroelectric coefficient was found to be strongly dependent on the choice of substrate material and film thickness. While the analysis in this article is focused on BST 60/40 and PZT 50/50, it is evident that such a methodology can very well be extended to other BST and PZT compositions and other ferroelectric thin films. Therefore, this work provides the basis for analyzing pyroelectric response of ferroelectric thin films and provides guidelines for choice of substrate and film thickness with respect to lattice parameter and TEC for obtaining optimum pyroelectric response.

One of the important conclusions of this article concerns the pyroresponse of ferroelectric films on Si substrates. Due to the large differences in both the lattice parameters and the TECs, ferroelectric films on Si will be highly influenced by extremely high in-plane tensile stresses. The effect of the difference in the TECs becomes more pronounced especially if the film growth is carried out at relatively high temperatures. Even for polycrystalline films on Si, thermal stresses alone should result in a variation in the phase transformation temperature, stabilizing the paraelectric phase, and thereby significantly reducing the pyroelectric response as shown in this report. This one-to-two orders of magnitude degradation in the pyroresponse poses a major challenge to any current and potential application of ferroelectrics as any device application requires integration with Si ICs. One way of reducing the effect of internal stresses is obviously by depositing one or more appropriately selected buffer layers as to “screen” the substrate from the film. The selection of the buffer layers should be chosen in such a way that the ferroelectric film should be in in-plane compression at the deposition temperature as to compensate for the tensile thermal stresses that will develop as the heterostructure is cooled to ambient temperatures. Therefore, in addition to the lattice parameter(s) of the buffer layer(s), the critical parameters that will eventually affect the stress state and the magnitude of the internal stresses in the film are the thickness(es) and the TEC(s) of the buffer layer(s).

## ACKNOWLEDGMENT

This work was supported by the National Science Foundation (NSF) under Grant No: DMR-0132918.

<sup>1</sup>R. Watton, *Ferroelectrics* **91**, 87 (1989).

<sup>2</sup>Björmander, K. Sreenivas, A. M. Grishin, and K. V. Rao, *Appl. Phys. Lett.* **67**, 58 (1995).

- <sup>3</sup>J.-G. Cheng, J. Tang, J.-H. Chu, and A.-J. Zhang, *Appl. Phys. Lett.* **77**, 1035 (2000).
- <sup>4</sup>A. Amin, *J. Electroceram.* **8**, 99 (2002).
- <sup>5</sup>M. E. Lines and A. M. Glass, *Principles and Applications of Ferroelectrics and Related Materials* (Clarendon, Oxford, 1977).
- <sup>6</sup>W.-G. Liu, J. S. Ko, and W.-G. Zhu, *Thin Solid Films* **371**, 254 (2000).
- <sup>7</sup>R. W. Whatmore, P. C. Osbond, and N. M. Shorrocks, *Ferroelectrics* **76**, 351 (1987).
- <sup>8</sup>B. M. Kulwicki, A. Amin, H. R. Beratan, and C. M. Hanson, *IEEE Proceedings on Application of Ferroelectrics*, Vol. 8(1) 1992.
- <sup>9</sup>T.-J. Zhang and H. Ni, *Sens. Actuators A* **100**, 252 (2002).
- <sup>10</sup>C. Shi, M. Liu, L. C. , Y. Zeng, and J. D. Costa, *Thin Solid Films* **375**, 288 (2000).
- <sup>11</sup>T. M. Shaw, S. Trolier-McKinstry, and P. C. McIntyre, *Annu. Rev. Mater. Sci.* **30**, 263 (2000).
- <sup>12</sup>V. Nagarajan, I. G. Jenkins, S. P. Alpay, S. Aggarwal, L. Salamanca-Riba, A. L. Roytburd, and R. Ramesh, *J. Appl. Phys.* **86**, 595 (1999).
- <sup>13</sup>V. Nagarajan, C. S. Ganpule, B. Nagaraj, S. Aggarwal, S. P. Alpay, A. L. Roytburd, E. D. Williams, and R. Ramesh, *Appl. Phys. Lett.* **75**, 4183 (1999).
- <sup>14</sup>V. Nagarajan, S. P. Alpay, C. S. Ganpule, B. Nagaraj, S. Aggarwal, E. D. Williams, A. L. Roytburd, and R. Ramesh, *Appl. Phys. Lett.* **77**, 438 (2000).
- <sup>15</sup>C. L. Canedy, H. Li, S. P. Alpay, L. Salamanca-Riba, A. L. Roytburd, and R. Ramesh, *Appl. Phys. Lett.* **77**, 1695 (2000).
- <sup>16</sup>Y. I. Yuzuk, P. Simon, I. N. Zakharchenko, V. A. Alyoshin, and E. V. Sviridov, *Phys. Rev. B* **66**, 052 103 (2002).
- <sup>17</sup>T. M. Shaw, Z. Suo, M. Huang, E. Liniger, R. B. Laibowitz, and J. D. Baniecki, *Appl. Phys. Lett.* **75**, 2129 (1999).
- <sup>18</sup>H. Li, A. L. Roytburd, S. P. Alpay, T. D. Tran, L. Salamanca-Riba, and R. Ramesh, *Appl. Phys. Lett.* **78**, 2354 (2001).
- <sup>19</sup>A. R. James and X. X. Xi, *J. Appl. Phys.* **92**, 6149 (2002).
- <sup>20</sup>A. L. Roytburd, S. P. Alpay, V. Nagarajan, C. S. Ganpule, S. Aggarwal, E. D. Williams, and R. Ramesh, *Phys. Rev. Lett.* **85**, 190 (2000).
- <sup>21</sup>C. S. Ganpule, A. Stanishevsky, S. Aggarwal, J. Melngailis, E. Williams, R. Ramesh, V. Joshi, and C. P. de Araujo, *Appl. Phys. Lett.* **75**, 3874 (1999).
- <sup>22</sup>N. A. Pertsev, A. G. Zembilgotov, and A. K. Tagantsev, *Phys. Rev. Lett.* **80**, 1988 (1998).
- <sup>23</sup>Z.-G. Ban and S. P. Alpay, *J. Appl. Phys.* **91**, 9288 (2002).
- <sup>24</sup>Z.-G. Ban and S. P. Alpay, *J. Appl. Phys.* **93**, 504 (2003).
- <sup>25</sup>N. A. Pertsev, V. G. Kukhar, H. Kohlstedt, and R. Waser, *Phys. Rev. B* **67**, 054 107 (2003).
- <sup>26</sup>Z.-G. Ban and S. P. Alpay, *Appl. Phys. Lett.* **82**, 3499 (2003).
- <sup>27</sup>*Landolt-Börnstein, Numerical Data and Functional Relationships in Science and Technology*, Vol. 16, edited by K.-H. Hellwege and A. M. Hellwege (Springer, Berlin, 1982).
- <sup>28</sup>B. Noheda, D. E. Cox, G. Shirane, J. A. Gonzalo, L. E. Cross, and S.-E. Park, *Appl. Phys. Lett.* **74**, 2059 (1999).
- <sup>29</sup>B. Noheda, J. A. Gonzalo, L. E. Cross, R. Guo, S.-E. Park, D. E. Cox, and G. Shirane, *Phys. Rev. B* **61**, 8687 (2000).
- <sup>30</sup>J. W. Matthews and A. E. Blakeslee, *J. Cryst. Growth* **27**, 118 (1974).
- <sup>31</sup>C. M. Foster, G.-. Bai, R. Csencsits, J. Vetrone, R. Jammy, L. A. Wills, E. Carr, and J. Amano, *J. Appl. Phys.* **81**, 2349 (1997).
- <sup>32</sup>L. P. Kadanoff, W. Gotze, D. Hamblen, R. Hecht, E. A. S. Lewis, V. V. Paiciauskas, M. Rayl, J. Swift, D. Aspnes, and J. Kane, *Rev. Mod. Phys.* **39**, 395 (1967); R. Kretschmer and K. Binder, *Phys. Rev. B* **20**, 1065 (1979).
- <sup>33</sup>The effects of systematic variations in the polarization distribution via compositional, temperature, and strain grading were treated theoretically in Z.-G. Ban, S. P. Alpay, and J. V. Mantese, *Phys. Rev. B* **67**, 184 104 (2003); S. P. Alpay, Z.-G. Ban, and J. V. Mantese, *Appl. Phys. Lett.* **82**, 1269 (2003).